J|A|C|S
COMMUNICATIONS

Published on Web 03/14/2006

Critical Properties of Aluminum

Divesh Bhatt, Ahren W. Jasper, Nathan E. Schultz, J. Ilja Siepmann,* and Donald G. Truhlar*

Department of Chemistry and Minnesota Supercomputing Institute, University of Minnesota, 207 Pleasant Street SE, Minneapolis, Minnesota 55455-0431

Received November 16, 2005; E-mail: siepmann@umn.edu; truhlar@umn.edu

Aluminum is one of the most ubiquitous elements on Earth. Since its isolation in 1825, aluminum has found many technological uses, but its physical properties are well-known only at low reduced temperature. In this work, Gibbs ensemble Monte Carlo calculations are performed using a validated embedded-atom potential to obtain the vapor−liquid coexistence curve and the critical properties for elemental aluminum. This demonstrates the ability of modern simulations to predict fundamental physical properties that are extremely difficult to measure directly.

Due to their strong cohesive interactions, the critical properties of most metals are not amenable to conventional experiments, and only the critical temperatures, T_c, of mercury and alkalis have been measured directly.[1] Estimates of T_c for other metals are based upon relationships between T_c and other measured thermodynamic properties. For Al, an analysis of isobaric expansion experiments[2] yields a value of 5726 K.[3] Another estimate, based upon the assumption that the entropies of vaporization of different metals are equal at the same reduced temperature, yields a value of 8550 K.[4] Renaudin et al.[3] compared new experimental data for pressure versus internal energy to two equations of state that extrapolate to T_c of ∼12 100 and ∼6400 K and obtained better agreement with the latter. Young and Alder[5] and Likalter[1] developed scaling laws based, respectively, on the van der Waals model and on the plasma-like behavior of metallic near-critical fluids and, respectively, estimated 7151 and 8860 K for T_c of Al.

Aluminum is of technological importance not only as a light-weight, rust-resistant structural material but also as an ingredient for high-energy fuels and, potentially, as a hydrogen storage device.[6] For many applications, such as the controlled growth of Al nanoparticles, precise knowledge of Al's saturated vapor pressure and heat of vaporization up to the critical point is pivotal. Furthermore, a technique for the creation of thin Al films is to first heat Al powder to a supercritical state and then spray a film onto a surface.[7] Thus, it is a serious concern that critical constants for Al are known with such poor precision. In cases where an experimental determination of the critical properties is difficult, molecular simulations using accurate potential energy functions offer a practical alternative.[8] However, the application of this technique to metals is usually impeded by insufficient knowledge of the potential energy function.[5]

Recently, some of us and co-workers[9,10] have presented the first validated potential energy function for a nanophase metal, in particular, nanoaluminum. That is, an analytic embedded-atom potential (called NP-B) was parametrized to reproduce accurate DFT energies for clusters and nanoparticles of various sizes,[10,11] a strategy made possible only by the development of reliable density functionals[12] that yield these data.

In the present report, we use the NP-B potential and, for comparison, a different embedded-atom potential (to be called MDEA)[13] that was fit only to bulk solid-state data for Al to calculate the vapor−liquid coexistence curve and critical parameters of Al from Gibbs ensemble Monte Carlo simulations.[14] Because of the large dimer binding energies of metal particles, aggregation-volume-bias Monte Carlo strategies[15] are used to efficiently sample cluster formation/breakage in the vapor phase and to establish the correct equilibrium distribution of clusters of different sizes. Configurational-bias Monte Carlo techniques[16,17] are used to enhance the acceptance rate for particle swaps between the two phases. Further details of the simulations are provided in the Supporting Information.

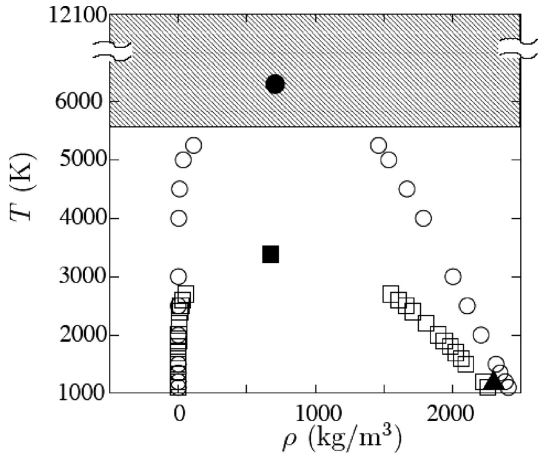

Figure 1. Vapor−liquid coexistence curves of Al calculated using the MDEA (squares) and NP-B (circles) potentials. The open and filled symbols denote the saturated densities and the estimated critical points, respectively. The shaded area represents the range of critical temperatures estimated from experimental data, and the filled triangle shows the experimental liquid density of molten Al at 1173 K.[18]

Figure 1 shows the temperature−density projection for the vapor−liquid coexistence curve of Al computed using the NP-B and MDEA potentials with the experimental liquid density at 1173 K[18] plotted for comparison. Most striking is the difference in the critical temperatures for NP-B ($T_c = 6299 \pm 48$ K) and MDEA ($T_c = 3381 \pm 13$ K). The latter estimate falls substantially below the lower end of experiment-based estimates for T_c. The corresponding values for the critical densities and pressures are $\rho_c = 707 \pm 60$ kg/m^3 and $p_c = 884 \pm 19$ atm for NP-B, and $\rho_c = 675 \pm 36$ kg/m^3 and $p_c = 435 \pm 20$ atm for MDEA. The error ranges given for calculated quantities arise from the sampling statistics (two standard deviations) and the extrapolation procedure used to determine the critical constants (see Supporting Information). This shows that the accuracy of the potential function and not the simulation protocol is the limiting factor in the reliability of these calculations. Figure 2 shows a Clausius−Clapeyron plot of the logarithm of the saturated vapor pressure versus the inverse temperature. At low temperature, the saturated vapor pressure for the MDEA potential falls substantially above the experimental estimate (which is based on measurement of the saturated vapor pressure, heat of vaporization, and heat capacity of the liquid phase at the triple point[19]), whereas the NP-B potential slightly under-

10.1021/ja0577950 CCC: $33.50

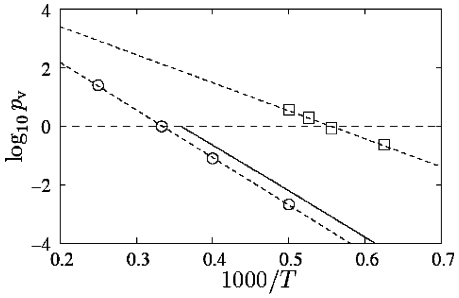

Figure 2. Clausius−Clapeyron plots for Al calculated using the MDEA (squares) and NP-B (circles) potentials. The short-dashed lines represent fits to the four data points surrounding standard pressure in units of atm. The experimental estimates[19] are shown as a solid line.

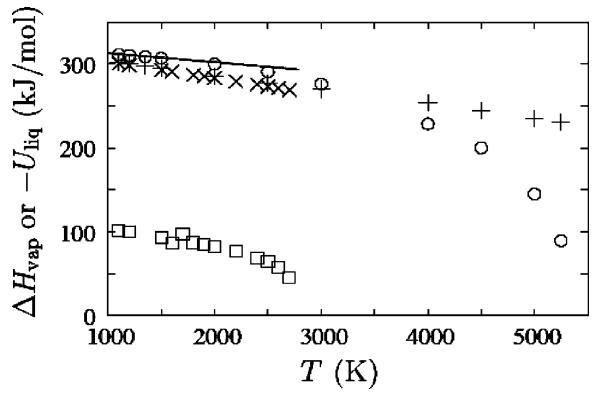

Figure 3. Heats of vaporization and internal energies of the liquid phase for Al calculated using the MDEA (squares for ΔH_{vap} and × symbols for $-U_{liq}$) and NP-B (circles for ΔH_{vap} and pluses for $-U_{liq}$) potentials. The experimental estimates[19] are shown as a solid line.

predicts the saturated vapor pressure but with a much smaller deviation. The corresponding estimates for the normal boiling point are 1802 ± 15 and 2993 ± 8 K for the MDEA and NP-B potentials, respectively, compared to the experimental value of $T_b = 2791$ K.[20] Thus the NP-B potential function overestimates the normal boiling point by 7%, and this also gives an estimate of the uncertainty of the NP-B potential for predicting the critical temperature.

Figure 3 compares the calculated heats of vaporization with the values obtained from low-temperature experimental data.[19] The NP-B potential yields ΔH_{vap} that agrees very well with the experimental data at low temperatures, where use of a constant specific heat is appropriate. In contrast, the MDEA potential underestimates ΔH_{vap} by a factor of 3. What can cause this apparent failure of the MDEA model fit to solid-state data? The low-temperature liquid densities are similar for both potentials and agree well with the experimental data (see Figure 1). However, the energetics for the two potentials in the vapor phase are rather different. For temperatures below its normal boiling point, the NP-B potential yields an internal energy of the liquid, U_{liq}, that differs in magnitude from ΔH_{vap} by an amount close to RT. In contrast, for the MDEA potential, U_{liq} is significantly larger in magnitude than ΔH_{vap}, that is, U_{vap} must be substantial in magnitude.

A cluster analysis for the vapor phase shows that at 1500 K for the NP-B potential, less than 0.2% of the atoms are involved in the formation of clusters, and the NP-B vapor deviates significantly from an ideal gas only at higher temperatures. In contrast, the MDEA vapor phase is very nonideal even at temperatures close to the experimental triple point; the vapor at 1500 K contains only 0.1% monomers.

In conclusion, an embedded-atom potential parametrized to accurate energies of nanoclusters is used to calculate the vapor−liquid equilibrium properties of Al. The results are satisfactory at low temperatures where experimental data are available. Al's saturated vapor phase behaves ideally for $T < 2000$ K, beyond which clustering in the vapor phase becomes appreciable—knowledge that is needed for the controlled growth of nanoparticles from the vapor phase. The critical temperature predicted by using this potential is close to 6300 K, near the lower end of the range of values (5700−12 100 K) extrapolated from experimental data. In this way, advances in computational material science are resolving fundamental questions about the physical properties of the elements that have remained too difficult for direct experimental measurement even 180 years after the isolation of the element.

Acknowledgment. We thank Marcus Martin for stimulating discussions. This work was supported in part by the National Science Foundation and by the Defense−University Research Initiative in Nanotechnology (DURINT) through a grant managed by the Army Research Office.

Supporting Information Available: A detailed description of the potential models, the simulation parameters, and analysis procedures, numerical results, and a plot of the compressibility factor. This material is available free of charge via the Internet at http://pubs.acs.org.

References

(1) Likalter, A. A. *Phys. Rev. B* **1996**, *53*, 4386.
(2) Gathers, G. R.; Ross, M. J. *Non-Cryst. Solids* **1984**, *61*−*62*, 59.
(3) Renaudin, P.; Blancard, C.; Clerouin, J.; Faussurier, G.; Noiret, P.; Recoules, V. *Phys. Rev. Lett.* **2003**, *91*, 75002/1.
(4) Grosse, A. V. J. *Inorg. Nucl. Chem.* **1962**, *24*, 147.
(5) Young, D. A.; Alder, B. J. *Phys. Rev. A* **1971**, *3*, 364.
(6) Zuttel, A.; Wenger, P.; Sudan, P.; Mauron, P.; Orimo, S. *Mater. Sci. Eng.* **2004**, *B108*, 9.
(7) Kim, J. K. Thin film coating of aluminum electrolytic condenser using supercritical aluminum. Korean Patent, KR 2000002085, Jan 15, 2000.
(8) Siepmann, J. I.; Karaborni, S.; Smit, B. *Nature* **1993**, *365*, 330.
(9) Jasper, A. W.; Staszewski, P.; Staszewska, G.; Schultz, N. E.; Truhlar, D. G. *J. Phys. Chem. B* **2004**, *108*, 8996.
(10) Jasper, A. W.; Schultz, N. E.; Truhlar, D. G. *J. Phys. Chem. B* **2005**, *109*, 3915.
(11) Schultz, N. E.; Staszewska, G.; Staszewska, P.; Truhlar, D. G. *J. Phys. Chem. B* **2004**, *108*, 4850.
(12) Adamo, C.; Barone, V. *J. Chem. Phys.* **1999**, *110*, 6158.
(13) Mei, J.; Davenport, J. W. *Phys. Rev. B* **1992**, *46*, 21.
(14) Panagiotopoulos, A. Z. *Mol. Phys.* **1987**, *61*, 813.
(15) Chen, B.; Siepmann, J. I. *J. Phys. Chem. B* **2000**, *104*, 8725.
(16) Siepmann, J. I.; Frenkel, D. *Mol. Phys.* **1992**, *75*, 59.
(17) Esselink, K.; Loyens, L. D. J. C.; Smit, B. *Phys. Rev. E* **1995**, *51*, 1560.
(18) Hatch, J. E. *Aluminum: Properties and Physical Metallurgy*; ASM: Metals Park, OH, 1984; Chapter 1.
(19) Hultgren, R. *Selected Values of the Thermodynamic Properties of the Elements*; ASM: Metals Park, OH, 1973.
(20) Chase, M. W., Jr. *J. Phys. Chem. Ref. Data* **1999**, *28*, Monograph 9.

JA0577950